Macromolecules

Article

pubs.acs.org/Macromolecules

ABC Triblock Copolymer Worms: Synthesis, Characterization, and Evaluation as Pickering Emulsifiers for Millimeter-Sized Droplets

C. J. Mable,[†] K. L. Thompson,[†] M. J. Derry,[†] O. O. Mykhaylyk,[†] B. P. Binks,[‡] and S. P. Armes*[,†]

[†]Department of Chemistry, University of Sheffield, Brook Hill, Sheffield S3 7HF, U.K.

[‡]School of Mathematics and Physical Sciences, University of Hull, Hull HU6 7RX, U.K.

Supporting Information

ABSTRACT: Polymerization-induced self-assembly (PISA) is used to prepare linear poly(glycerol monomethacrylate)−poly(2-hydroxypropyl methacrylate)−poly(benzyl methacrylate) [PGMA−PHPMA−PBzMA] triblock copolymer nano-objects in the form of a concentrated aqueous dispersion via a three-step synthesis based on reversible addition−fragmentation chain transfer (RAFT) polymerization. First, GMA is polymerized via RAFT solution polymerization in ethanol, then HPMA is polymerized via RAFT aqueous solution polymerization, and finally BzMA is polymerized via "seeded" RAFT aqueous emulsion polymerization. For certain block compositions, highly anisotropic worm-like particles are obtained, which are characterized by small-angle X-ray scattering (SAXS) and transmission electron microscopy (TEM). The design rules for accessing higher order morphologies (i.e., worms or vesicles) are briefly explored. Surprisingly, vesicular morphologies cannot be accessed by targeting longer PBzMA blocks—instead, only spherical nanoparticles are formed. SAXS is used to rationalize these counterintuitive observations, which are best explained by considering subtle changes in the relative enthalpic incompatibilities between the three blocks during the growth of the PBzMA block. Finally, the PGMA−PHPMA−PBzMA worms are evaluated as Pickering emulsifiers for the stabilization of oil-in-water emulsions. Millimeter-sized oil droplets can be obtained using low-shear homogenization (hand-shaking) in the presence of 20 vol % *n*-dodecane. In contrast, control experiments performed using PGMA−PHPMA diblock copolymer worms indicate that these more delicate nanostructures do not survive even these mild conditions.

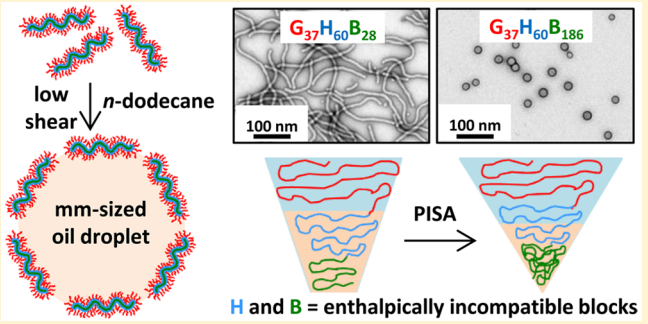

INTRODUCTION

Particle-stabilized emulsions, otherwise known as Pickering emulsions, have been recognized for more than a century.[1] Many classes of particles including silica,[2−6] polymer latexes,[6−10] and clays[11−14] can be used to stabilize such emulsions, with surface wettability usually dictating the emulsion type. Thus relatively hydrophilic particles tend to favor the formation of oil-in-water (o/w) emulsions, whereas relatively hydrophobic particles usually produce water-in-oil (w/o) emulsions.[15−17] Over the past decade or so, increasing attention has been paid to the use of highly anisotropic particles. For example, Noble et al. reported the use of polymeric microrods to prepare water-in-oil emulsions and ultimately colloidosomes.[18] More recently, Kalashnikova et al. evaluated various types of cellulose-based Pickering emulsifiers of ribbon-like shape.[19−21] Similarly, Wege et al.[22] utilized hydrophobic anisotropic cellulose microparticles to stabilize water-in-oil emulsions. Vermant and co-workers[23] employed a multiple backscattering technique to demonstrate that more stable Pickering emulsions are obtained when employing ellipsoidal polystyrene latexes (mean aspect ratio ∼9) compared to conventional spherical latex particles. Similar results were also reported for ellipsoidal hematite particles (mean aspect ratio ∼6).[23]

Over the past decade, we and others have utilized polymerization-induced self-assembly (PISA) to prepare a wide range of diblock copolymer nano-objects of tunable size, shape, and surface chemistry in the form of concentrated colloidal dispersions.[24−28] Of particular relevance to the present work, PISA provides an extremely attractive route to highly anisotropic block copolymer worms,[29] enabling their synthesis on a multigram scale in either polar solvents (e.g., water[24,30] or ethanol[25,31]) or non-polar solvents (e.g., *n*-alkanes[32,33]). Reproducible PISA syntheses of such worms usually require the construction of phase diagrams,[34,35] although *ad hoc* syntheses can sometimes also be effective.[36] Recently, we compared the performance of hydrophilic *linear* and cross-linked poly(glycerol monomethacrylate)-poly(2-hydroxypropyl methacrylate) [PGMA−PHPMA] diblock copolymer worms prepared via PISA in aqueous solution as Pickering emulsifiers for the production of o/w emulsions.[36] The linear worms did

Received: August 8, 2016
Revised: September 21, 2016
Published: October 5, 2016

DOI: 10.1021/acs.macromol.6b01729
Macromolecules 2016, 49, 7897−7907

not survive the high-energy homogenization conditions required to generate the oil droplets: instead, worm dissociation occurs to generate individual copolymer chains, which then act as a polymeric surfactant to stabilize the emulsion. However, the corresponding *cross-linked* worms (which were obtained via addition of a small amount of ethylene glycol dimethacrylate) survived homogenization, leading to the formation of genuine Pickering emulsions. In related work, hydrophobic linear poly(lauryl methacrylate)−poly(benzyl methacrylate) [PLMA−PBzMA] worms prepared via PISA in *n*-dodecane survived homogenization to produce w/o Pickering emulsions.[16] In this case the worms exhibited thermoresponsive behavior: heating to 150 °C led to a worm-to-sphere transition that was essentially irreversible if it is conducted in sufficiently dilute solution (1.0% w/w). Thus this system provided a unique opportunity to compare the effect of particle morphology on Pickering emulsifier performance for *chemically identical* spheres and worms.[16] It was found that the worms were more effective stabilizers because they produced finer, more stable oil droplets than the spheres when directly compared under the same conditions. This is understandable because worms are 1−2 orders of magnitude more strongly adsorbed at the oil−water interface than spheres, yet have a comparable surface area per unit mass, A_s (the A_s for highly anisotropic worms is estimated to be only approximately 33% less than the A_s for the corresponding spheres).[16,36] Given these intrinsic advantages, and the relative ease with which block copolymer worms can now be accessed via PISA syntheses, further exploration of the use of such anisotropic particles as Pickering emulsifiers is clearly warranted.

In this work, we revisit our recent empirical (and serendipitous) discovery that *linear* PGMA−PHPMA−PBzMA triblock copolymers can form sufficiently robust worms to act as Pickering emulsifiers for o/w emulsions.[36] More specifically, we examine the scope and limitations of the PISA synthesis of such worms, explain why the copolymer morphology does not evolve further to produce vesicles, characterize the worm dimensions using transmission electron microscopy (TEM) and small-angle X-ray scattering (SAXS), and assess the performance of such worms as hydrophilic Pickering emulsifiers for the production of millimeter-sized oil droplets.

RESULTS AND DISCUSSION

Synthesis and Characterization of Block Copolymers.

For the sake of brevity, a shorthand notation is utilized throughout this article to describe the various block copolymers. Thus G, H, and B are used to represent glycerol monomethacrylate (GMA), 2-hydroxypropyl methacrylate (HPMA), and benzyl methacrylate (BzMA), respectively. Hence $G_xH_yB_z$ denotes poly(glycerol monomethacrylate-*block*-2-hydroxypropyl methacrylate-*block*-benzyl methacrylate), where *x*, *y*, and *z* indicate the mean degrees of polymerization (DP) of the three respective blocks.

The initial RAFT solution polymerization of GMA was conducted in ethanol at 70 °C to generate a near-monodisperse G_{37} macromolecular chain transfer agent (macro-CTA) (M_w/M_n = 1.19; see Figure S1 and Table 1). After purification, this water-soluble macro-CTA was utilized for the *in situ* RAFT aqueous solution polymerization of HPMA at 15% w/w solids, yielding a 100 g batch of $G_{37}H_{60}$ diblock copolymer precursor (see Figure 1a). ^{1}H NMR studies indicated that more than 99% HPMA conversion was achieved within 2 h at 70 °C (see Figure S2), as expected from previous studies.[34] Gel permeation chromatography (GPC) studies indicated that a near-monodisperse diblock copolymer was obtained with high blocking efficiencies and minimal macro-CTA contamination (M_w/M_n = 1.14; see Figure S1 and Table 1). The GPC trace was unimodal but a high molecular weight shoulder was discernible, which has been attributed to low levels of dimethacrylate impurity in the HPMA monomer (approximately 0.07 mol % as judged by HPLC analysis); this results in light branching of the PHPMA chains. Dynamic light scattering (DLS) studies of this $G_{37}H_{60}$ diblock copolymer reveal a relatively low count rate of 50 kcps, and ^{1}H NMR studies confirm that the PHPMA block is fully soluble in water (see Figure S3), suggesting that self-assembly does not occur for this relatively short PHPMA block.

Table 1. Summary of ^{1}H NMR-Derived Monomer Conversion, Apparent DLS Hydrodynamic Diameter (D_h) and Polydispersity, Number-Average Molecular Weight (M_n), and Polydispersity (M_w/M_n) Determined for a G_{37} Macro-CTA, a $G_{37}H_{60}$ Diblock Copolymer Precursor, a Series of Seven $G_{37}H_{60}B_z$ Triblock Copolymers (Where *z* Ranges from 10 to 550), a $G_{37}H_{90}$ Diblock Copolymer Control, a G_{92} Macro-CTA Precursor, and a $G_{92}B_{28}$ Diblock Copolymer Control

Copolymer Composition	BzMA conv/%	D_h (PDI)[c] /nm	M_n[b] / g mol^{-1}	M_w/M_n[b]
G_{37} macro-CTA			9800	1.19
$G_{37}H_{60}$	>99[a]	119 (0.31)	20200	1.14
$G_{37}H_{60}B_{10}$	98	41 (0.13)	21000	1.13
$G_{37}H_{60}B_{28}$	94	147 (0.23)	22600	1.13
$G_{37}H_{60}B_{47}$	95	79 (0.16)	24300	1.14
$G_{37}H_{60}B_{92}$	92	45 (0.03)	29300	1.16
$G_{37}H_{60}B_{186}$	93	63 (0.04)	39300	1.18
$G_{37}H_{60}B_{300}$	>99	86 (0.14)	50500	1.17
$G_{37}H_{60}B_{550}$	>99	120 (0.06)	69500	1.19
$G_{37}H_{90}$	>99[a]	46 (0.13)	25500	1.11
G_{92} macro-CTA			23900	1.12
$G_{92}B_{28}$	94	28 (0.36)	26300	1.14

[a]Data correspond to HPMA conversion, rather than BzMA conversion. [b]DMF GPC data recorded using a refractive index detector and calibrated using a series of poly(methyl methacrylate) standards. [c]D_h is a *sphere-equivalent* diameter in the case of worms.

Furthermore, no nanoparticles can be observed by TEM (see image in Figure 2), which again indicates that the PHPMA block is not sufficiently long to induce micellar nucleation. This is consistent with observations made by Blanazs and coworkers, who found that a minimum PHPMA DP of around 90 was required to induce nucleation when using a $PGMA_{47}$ macro-CTA.[34] However, it should be noted that this minimum critical DP is expected to be rather sensitive to the precise PISA formulation.[37]

This $G_{37}H_{60}$ diblock copolymer precursor was then utilized as a macro-CTA for the RAFT seeded emulsion polymerization of BzMA at 70 °C to produce a series of seven $G_{37}H_{60}B_z$ triblock copolymers, where *z* ranged from 10 to 550 (see Figure 1a). ^{1}H NMR studies confirmed that BzMA conversions greater than 92% were obtained in each case (see Figure S2 and Table 1). Dimethylformamide (DMF) GPC studies indicated that near-monodisperse triblock copolymers were obtained (M_w/M_n < 1.20, see Table 1) with high blocking efficiencies (see Figure

DOI: 10.1021/acs.macromol.6b01729
Macromolecules 2016, 49, 7897−7907

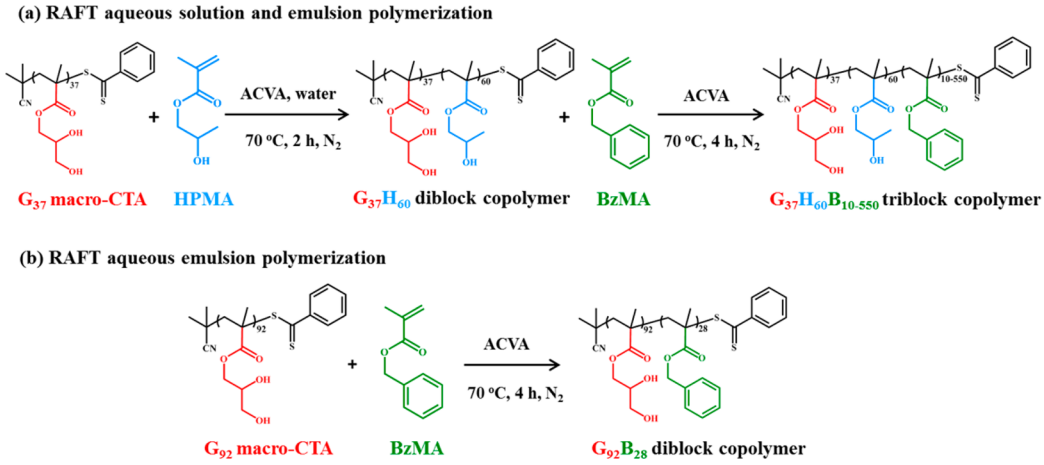

Figure 1. Synthesis of (a) $G_{37}H_{60}B_{10-550}$ triblock copolymer via RAFT aqueous solution polymerization of HPMA followed by RAFT seeded emulsion polymerization of BzMA and (b) $G_{92}B_{28}$ diblock copolymer prepared via RAFT aqueous emulsion polymerization of BzMA.

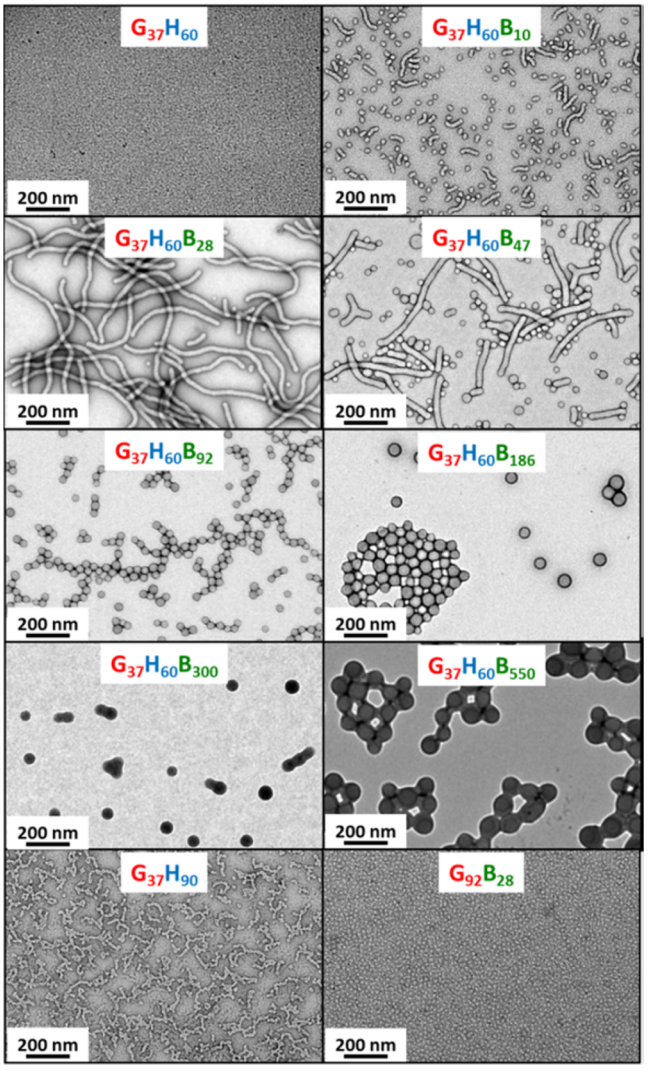

Figure 2. TEM images obtained for dried dilute aqueous dispersions of the $G_{37}H_{60}$ diblock copolymer precursor, a series of seven $G_{37}H_{60}B_z$ triblock copolymers (where z ranges from 10 to 550), the $G_{37}H_{90}$ diblock copolymer worms, and the $G_{92}B_{28}$ diblock copolymer spheres.

S1). TEM images shown in Figure 2 and DLS studies (see Table 1) indicated that spheres with a hydrodynamic diameter (D_h) of 41 nm were formed when z = 10; thus chain extension with just 10 units of BzMA is sufficient to induce micellar nucleation. When targeting a PBzMA DP of 30 (and achieving a DP of 28), TEM studies indicated the formation of highly anisotropic worms (Figure 2), similar to those reported recently.[36]

These $G_{37}H_{60}B_{28}$ worms were further characterized by SAXS. The worm model[38−40] provided an excellent fit to the SAXS pattern over six orders of magnitude of X-ray scattering intensity (see Figure S4a). The mean worm contour length (L_w) was determined to be 653 nm, which is consistent with TEM observations. Assuming a circular worm cross-section, the mean worm width (W_w), was calculated to be 25.6 ± 1.7 nm, which is also consistent with that estimated from TEM images (for which W_w = 24.2 ± 3.2 nm), where $W_w = 2R_{sw} + 4R_g$, with R_{sw} representing the radius of the worm core cross section and R_g representing the radius of gyration of the corona chains. The R_g of the G_{37} corona block of these worms was determined to be 1.7 nm from the data fit to the SAXS pattern (see Figure 4a). This experimental value is comparable to a theoretical estimate: the projected contour length of a single GMA monomer is 0.255 nm (two carbon bonds in an *all-trans* conformation), the total contour length of a G_{37} block, L_{PGMA} = 37 × 0.255 nm = 9.44 nm, and the literature value of the Kuhn length for poly(methyl methacrylate) is 1.53 nm,[41] resulting in an R_g of $(9.44 \times 1.53/6)^{1/2}$, or 1.55 nm. A worm model fit to the SAXS data pattern of $G_{37}H_{60}B_{28}$ (Figure S4a) indicated that the solvent volume fraction in the core (x_{sol}) is 0.03, which suggests that the hydrophobic worm cores are essentially non-solvated. This is significantly different to x_{sol} values reported recently by Warren et al.[28] for $G_{55}H_y$ diblock copolymer vesicles, which ranged from 0.38 to 0.66 as y was increased from 200 to 1000. It is evident that extension with approximately 28 units of BzMA not only changes the nanoparticle morphology from spheres to worms but also drastically changes the extent of hydration of the nanoparticle cores.

Based on the PISA literature,[37,42−45] it was anticipated that vesicular morphologies should be obtained for these $G_{37}H_{60}B_z$ triblock copolymers as the target DP of the PBzMA block was gradually increased. However, only branched worms and spheres were obtained when z = 47 (see TEM images in Figure 2). Furthermore, both TEM and DLS studies indicated that only spheres were obtained when $z \geq 92$ (see Figure 2 and Table 1, respectively). The spheres progressively increase in

DOI: 10.1021/acs.macromol.6b01729
Macromolecules 2016, 49, 7897−7907

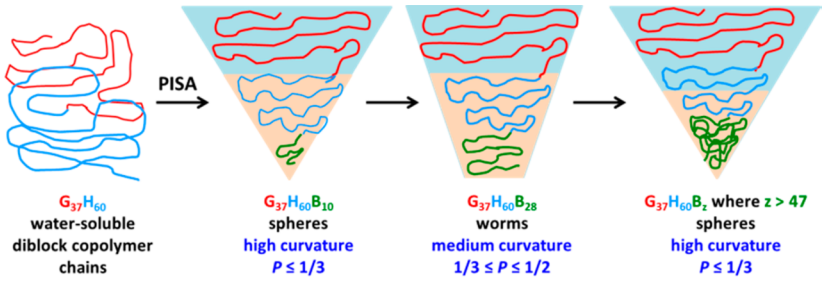

Figure 3. Schematic cartoon to illustrate the conformational behavior of $G_{37}H_{60}B_z$ triblock copolymer chains as z is systematically increased. Hydrophilic regions are represented by blue and hydrophobic regions are represented by orange. The packing parameter, P, is given by $P = v/a_o l_c$ where v is the volume of the hydrophobic chains, a_o is the optimal area of the head-group, and l_c is the length of the hydrophobic tail.[42,48] Initially, the $G_{37}H_{60}$ diblock copolymer precursor chains are molecularly dissolved in the aqueous phase. For $z \sim 10$, the relatively short PBzMA block induces nucleation, producing spherical micelles with mixed cores comprising the $PHPMA_{60}$ and the $PBzMA_{10}$ blocks. For $z \sim 30$, the growing PBzMA block leads to an increase in P, which drives a sphere-to-worm transition during PISA. When $z \sim 47$, the PHPMA block becomes at least partly co-located within the stabilizer corona layer, rather than the core. This is because the weakly hydrophobic PHPMA block is actually less enthalpically incompatible with the hydrophilic PGMA block than with the highly hydrophobic PBzMA block. This inevitably causes a reduction in P, which leads to a worm-to-sphere transition.

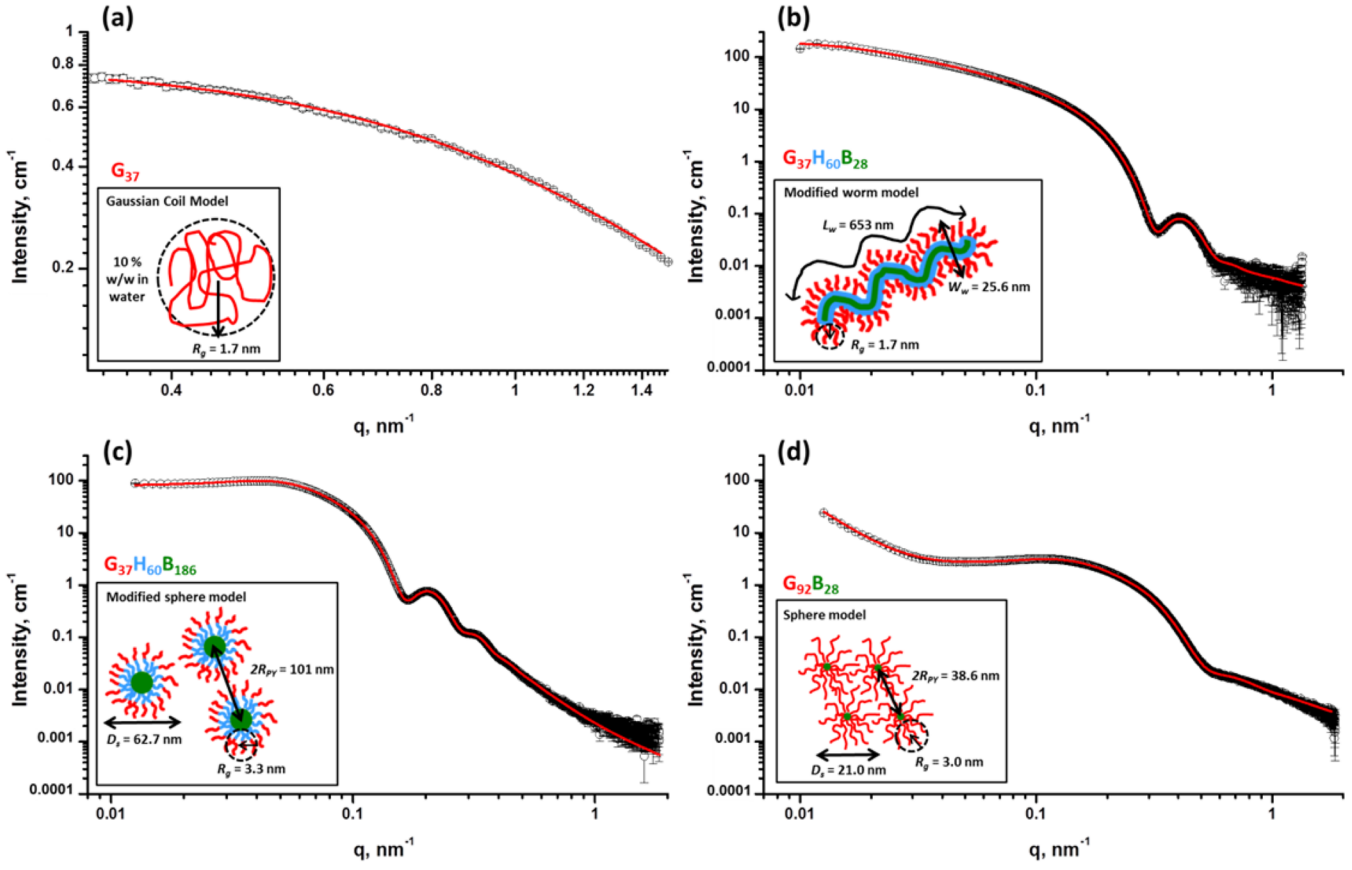

Figure 4. SAXS data (open black circles) and fits (red lines) for (a) a G_{37} macro-CTA and dilute aqueous dispersions of (b) $G_{37}H_{60}B_{28}$ triblock copolymer worms, (c) $G_{37}H_{60}B_{186}$ triblock copolymer spheres, and (d) $G_{92}B_{28}$ diblock copolymer spheres. Insets: schematic cartoons of the corresponding morphologies, where L_w = the contour length of the worm, W_w = width of the worm, R_g = radius of gyration, D_s = diameter of the sphere, and R_{PY} = Percus−Yevick correlation radius of densely packed spheres (see Table S1). Note: structural morphologies are not drawn to scale. SAXS data were collected at (a) University of Sheffield and (b−d) Diamond Light Source (Didcot, UK).

mean diameter from 45 to 120 nm as z was systematically varied from 92 to 550, but vesicular morphologies were never obtained. Hypothetically, the spherical morphology observed by TEM might actually correspond to small vesicles. However, the SAXS pattern recorded for the $G_{37}H_{60}B_{186}$ triblock copolymer has a gradient that tends to zero at low q (see Figure S4b), indicating typical spherical particles[46] rather than hollow spheres (or vesicles). Analysis of the $G_{37}H_{60}B_{186}$ SAXS pattern using a spherical micelle model[38−40,47] gave an excellent data fit over six orders of magnitude of X-ray scattering intensity (Figure S4b). The SAXS-derived mean sphere diameter (D_s) was calculated to be 56.2 ± 5.4 nm, which is similar to that reported by DLS (63 nm, see Table 1). The structure factor peak observed in the SAXS pattern at $q \sim 0.05$ nm^{-1} (Figure S4b) suggests that the spheres are weakly aggregated. The Percus−Yevick correlation radius of packed

DOI: 10.1021/acs.macromol.6b01729
Macromolecules 2016, 49, 7897−7907

spheres (R_{PY}) was obtained to be 50.5 nm. The TEM images obtained for dispersions when $z \geq 92$ also show that the spheres may be partially fused/weakly aggregated. However, the number-average diameter estimated from TEM images recorded for $G_{37}H_{60}B_{92-550}$ triblock copolymer spheres corresponds quite closely to the hydrodynamic diameter obtained from DLS studies (see entries 6–9 in Table 1).

Although these results are somewhat counterintuitive when compared to most of the recent PISA literature,[37,42−45] it is perhaps not too surprising that only spheres are obtained when targeting higher DPs for the PBzMA block. For example, Cunningham et al.[27] prepared a series of $G_{51}B_y$ diblock copolymer spheres via RAFT aqueous emulsion polymerization of BzMA, with y ranging from 50 to 1000. Only spherical nanoparticles were obtained in all cases, regardless of the total solids content. In the present study, a weakly hydrophobic PHPMA block lies between the hydrophilic PGMA and highly hydrophobic PBzMA blocks, which allows triblock copolymer worms to be prepared for compositions containing just 31 mol % PBzMA. However, targeting higher PBzMA contents only leads to the formation of triblock copolymer spheres. The most likely explanation for these unexpected observations is that the PBzMA block is enthalpically highly incompatible with the PHPMA block, whereas the PHPMA block is only rather weakly incompatible with the PGMA block. Thus, when the $G_{37}H_{60}$ diblock copolymer is chain-extended with BzMA, at least some fraction of the partially hydrated PHPMA block[24] is gradually driven out of the increasingly hydrophobic core to become co-located with the PGMA stabilizer chains in the hydrophilic corona (see the schematic cartoon shown in Figure 3). If this is the case, it would lead to an effectively longer stabilizer block, with a theoretical maximum DP of 97 (i.e., the sum of G_{37} and H_{60}).

SAXS analysis allows this hypothesis to be examined.[49] A SAXS pattern was collected for a 10% w/w aqueous solution of the G_{37} macro-CTA (i.e., for molecularly dissolved chains below their overlap concentration). A satisfactory data fit was obtained for this pattern using a Gaussian coil model,[50] which indicated a R_g of 1.7 nm (see Figure 4a). This is very close to the R_g value for the stabilizer chains obtained from fitting the $G_{37}H_{60}B_{28}$ SAXS pattern using the worm model (see Table S1). This suggests that all of the weakly hydrophobic $PHPMA_{60}$ blocks are located within the core of the worms, while the hydrophilic $PGMA_{37}$ blocks occupy the worm corona. To test this hypothesis, the worm model was slightly modified (see SAXS models given in the Supporting Information) by incorporating an additional fitting parameter (η) corresponding to the volume fraction of the PHPMA block within the core domain. This η parameter enables the volume of the core and corona to be determined, rather than fixing these values based on the known block compositions. By definition, if the whole PHPMA block is located within the core, η should be equal to unity. In contrast, η should be zero if the PHPMA block is solely located in the corona. A good data fit was obtained for the $G_{37}H_{60}B_{28}$ SAXS pattern using the modified worm model (see Figure 4b). The fitting parameters were similar to those obtained when using the unmodified, original worm model (see Table S1). The R_g for the G_{37} corona block of this triblock copolymer was determined to be 1.7 nm, which is identical to that obtained for the G_{37} macro-CTA alone (see Figure 4a). Moreover, η tends toward unity, indicating that all of the PHPMA block is located in the worm core (see Figure 3).

A spherical micelle model[38−40,47] was similarly modified by incorporating η as an additional fitting parameter (see SAXS models and Table S1). Analysis of the $G_{37}H_{60}B_{186}$ spheres using this more sophisticated model gave a reasonably good data fit to the SAXS pattern over six orders of magnitude of X-ray scattering intensity (Figure 4c). Again, the fitting parameters were similar to those obtained when using the original unmodified sphere model (see Table S1). However, the R_g of the G_{37} corona block for this $G_{37}H_{60}B_{186}$ triblock copolymer was determined to be 3.3 nm from this analysis, which is significantly larger than that obtained for the $G_{37}H_{60}B_{28}$ worms. Notwithstanding the imperfect data fit at high q, this indicates that the stabilizer corona is somewhat thicker in the former case, even though the *same* $G_{37}H_{60}$ *diblock precursor* was used for the PISA synthesis of the $G_{37}H_{60}B_{28}$ and $G_{37}H_{60}B_{186}$ triblocks. Moreover, η was found to be 0.62, which suggests that a significant fraction of the PHPMA block is now located in the corona, rather than in the core (see Figure 3). This provides direct experimental evidence for a higher effective DP for the corona block when targeting a longer PBzMA core-forming block. For the $G_{37}H_{60}B_{186}$ triblock copolymer spheres, SAXS analysis indicates that around 23 HPMA repeat units $[(1 - 0.62) \times 60 \approx 23]$ in each PHPMA block are located within the corona, while the remaining 37 repeat units occupy the core along with the PBzMA chains. This increase in the effective stabilizer block DP leads to a reduction in the packing parameter, P, which in turn causes the observed worm-to-sphere transition (see Figure 3). The driving force for relocating approximately one-third of the PHPMA block within the corona is the greater incompatibility within the PHPMA and PBzMA blocks as the DP of the PBzMA block is increased. In this context, Mable et al.[51] recently reported that systematically varying the PBzMA block DP (or z) from 25 to 400 led to an evolution in framboidal morphology for a series of $G_{63}H_{350}B_z$ triblock copolymer vesicles. Thus it is not really surprising that enthalpic demixing between the PHPMA and PBzMA blocks leads to a dramatic change in morphology in the present work. In summary, SAXS provides useful insight into the unusual (and at first sight counterintuitive) evolution in copolymer morphology for this particular PISA formulation, which can be rationalized by considering subtle changes in the relative enthalpic incompatibilities between the three blocks during the growth of the PBzMA core-forming block.

In order to examine whether the intermediate PHPMA block is really essential for worm formation, a $G_{92}B_{28}$ diblock copolymer was synthesized via RAFT aqueous emulsion polymerization of BzMA using a G_{92} macro-CTA (see Figure 1b). The G_{92} block was designed to have a comparable DP to that of the combined DP of the G_{37} and H_{60} blocks, while a PBzMA DP of 30 was targeted because this produced worms for the ABC triblock formulation. ^{1}H NMR studies indicated that 94% BzMA conversion was achieved after 4 h at 70 °C (see Figure S5). GPC studies indicated that a low-polydispersity diblock copolymer was obtained with a high blocking efficiency and minimal macro-CTA contamination (M_w/M_n = 1.14; see Figure S6 and Table 1). DLS studies indicate a mean D_h of 28 nm (see Table 1). TEM images confirmed the formation of very small spheres of around 11.3 ± 2.5 nm diameter (based on analyzing 100 nanoparticles) with no evidence for the presence of any worms (see Figure 2). SAXS analysis confirmed that spheres are indeed formed because the gradient of the SAXS pattern tends to zero in the low q region, which is characteristic of spheres.[46] Analysis of this SAXS pattern using a star-like

DOI: 10.1021/acs.macromol.6b01729
Macromolecules 2016, 49, 7897−7907

micelle model[47,52] provided a satisfactory data fit over five orders of magnitude of X-ray scattering intensity (see Figure 4d). The mean sphere diameter, D_s, was calculated to be 21.0 ± 1.4 nm, which is comparable to that suggested by DLS, while the R_g of the G_{92} corona block for this $G_{92}B_{28}$ diblock copolymer was determined to be 3.0 nm. This experimental value is larger than the theoretical estimate (where R_g was calculated to be 2.45 nm) due to the star-like nature of the spheres. The spherical core diameter was determined to be 9.0 ± 1.4 nm, which is comparable to that estimated from TEM images. The correlation radius for densely packed spheres, R_{PY}, was determined to be 19.3 nm. This is simply a consequence of the star-like nature of the former copolymer,[47,53] which has a much higher effective volume fraction and hence a significantly lower critical overlap concentration. There is a pronounced upturn in the X-ray scattering intensity at low q (below 0.017 nm^{-1}; see Figure 4d). This could indicate the formation of aggregates (or mass fractals) most likely due to the extensive overlap between stabilizer chains of the micelles. The formation of spherical star-like micelles by this $G_{92}B_{28}$ diblock copolymer suggests that an intermediate PHPMA block is an essential prerequisite for obtaining a worm morphology. A reasonable explanation for this unexpected observation is outlined in Figure 3.

Millimeter-Sized Pickering Emulsion Droplets. Recently, Thompson et al. reported that $G_{45}H_{200}$ diblock copolymer vesicles were unstable with respect to dissociation when used as a Pickering emulsifier. However, chemical cross-linking of such vesicles using ethylene glycol dimethacrylate as a third block dramatically improved their stability toward high-shear homogenization: TEM studies of dried emulsion droplets confirmed that such covalently stabilized vesicles were adsorbed intact at the oil−water interface.[54] More recently, Thompson et al. reported that $G_{45}H_{140}$ diblock copolymer worms similarly could not withstand high-shear homogenization, whereas $G_{37}H_{60}B_{30}$ triblock copolymer worms proved to be highly efficient Pickering emulsifiers.[36] Moreover, DLS studies showed that the former worms were thermoresponsive, as expected based on previous work by Verber et al.[30] In contrast, the $G_{37}H_{60}B_{30}$ triblock copolymer worms were not thermoresponsive; this indicates that introducing the more hydrophobic PBzMA block stabilizes the worm morphology. In the present study, we have used RAFT aqueous dispersion polymerization (see Figure 1a) to prepare $G_{37}H_{90}$ diblock copolymer worms, which were designed to be analogous to the $G_{37}H_{60}B_{28}$ triblock copolymer worms. ^{1}H NMR studies confirmed that more than 99% HPMA conversion was achieved after 2 h at 70 °C (see Figure S7). GPC studies indicated that a near-monodisperse diblock copolymer was obtained with a high blocking efficiency and minimal macro-CTA contamination (M_w/M_n = 1.11; see Figure S8 and Table 1). DLS studies (see Table 1) and TEM images (see Figure 2) were consistent with the targeted pure worm morphology. Rheology experiments for the $G_{37}H_{60}B_{28}$ triblock copolymer worm gel were performed at 1.0% strain using an angular frequency of 1.0 rad s^{-1} (see Figure S9). Figure 5 shows the minimal change in gel moduli for this dispersion during a 25 °C to 2 °C to 25 °C thermal cycle. These $G_{37}H_{60}B_{28}$ worms proved to be non-thermoresponsive, with a G' of approximately 400 Pa being maintained over the entire temperature range.

Incorporating the highly hydrophobic PBzMA block enables the $G_{37}H_{60}B_{28}$ worms to act as an effective Pickering emulsifier. Previously, we reported that $G_{37}H_{60}B_{28}$ worms can survive the high-shear homogenization conditions required for emulsification, whereas $G_{45}H_{140}$ worms undergo dissociation to form individual copolymer chains under these conditions.[36] In the present study, we examined homogenization under much lower shear conditions, i.e., hand-shaking.

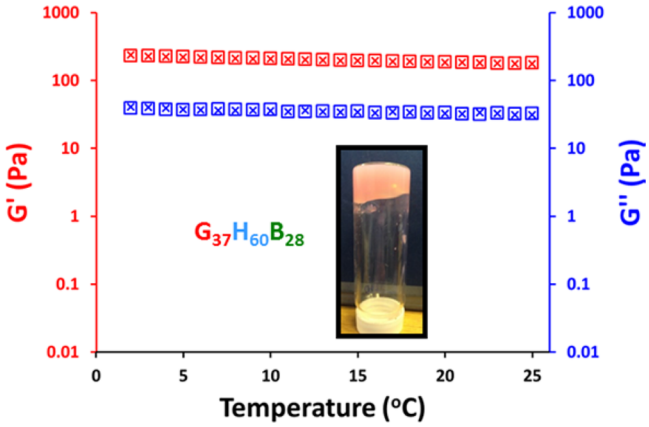

Figure 5. Variation of storage moduli (G', red) and loss moduli (G'', blue) for a $G_{37}H_{60}B_{28}$ triblock copolymer worm gel at 13% w/w during temperature cycling at 1 °C min^{-1} with 5 min equilibration at each temperature: (i) cooling from 25 to 2 °C (G' = open red squares, G'' = open blue squares) and (ii) subsequent warming from 2 to 25 °C (G' = red crosses, G'' = blue crosses). Inset: digital image of the worm gel at 20 °C during the tube inversion test. Measurements conducted using oscillatory mode at 1 rad s^{-1} angular frequency and 1% strain amplitude.

More specifically, both $G_{37}H_{60}B_{28}$ and $G_{37}H_{90}$ worms were evaluated as putative Pickering emulsifiers for the stabilization of *n*-dodecane emulsion droplets in water. Aqueous worm dispersions (1.88×10^{-3} to 1.00% w/w) were hand-shaken with 20 vol % *n*-dodecane for 2 min at 20 °C to produce emulsions. In order to examine whether the worms were adsorbed intact at the oil−water interface, optical microscopy (OM) and laser diffraction were used to determine the mean oil droplet diameters (see Figure 6). According to OM studies, the oil droplets became larger as the $G_{37}H_{60}B_{28}$ worm concentration was lowered, as shown in Figure 6a. These observations were corroborated by laser diffraction studies: the mean oil droplet diameter increased from 115 to 483 μm as the worm dispersion concentration was reduced from 1.00 to 0.0075% w/w (see Figure 6c). This concentration-dependent behavior is consistent with the formation of genuine Pickering emulsions (see Figure 7).[5,55−57] This was expected because Thompson et al. recently reported that such triblock copolymer worms can withstand high-shear homogenization, so they should also survive low-shear homogenization.[36] It is worth emphasizing that the mean oil droplet diameters are much larger when using hand-shaking for emulsification (approximately 115 μm at 1.00% w/w) compared to those obtained using high-shear homogenization (approximately 45 μm at 1.00% w/w).[36] When the worm dispersion concentration was lowered to 1.88×10^{-3} % w/w, the oil droplets proved to be too unstable to be assessed by laser diffraction. However, the droplet diameter was estimated (from digital photographs recorded immediately after emulsification) to be 1.11 ± 0.42 mm (based on measuring 120 droplets). Droplet coalescence occurs within a few hours, but reconstitution of the original emulsions could be achieved via further hand-shaking. This differs from the highly stable millimeter-sized emulsions prepared using partially hydro-

DOI: 10.1021/acs.macromol.6b01729
Macromolecules 2016, 49, 7897−7907

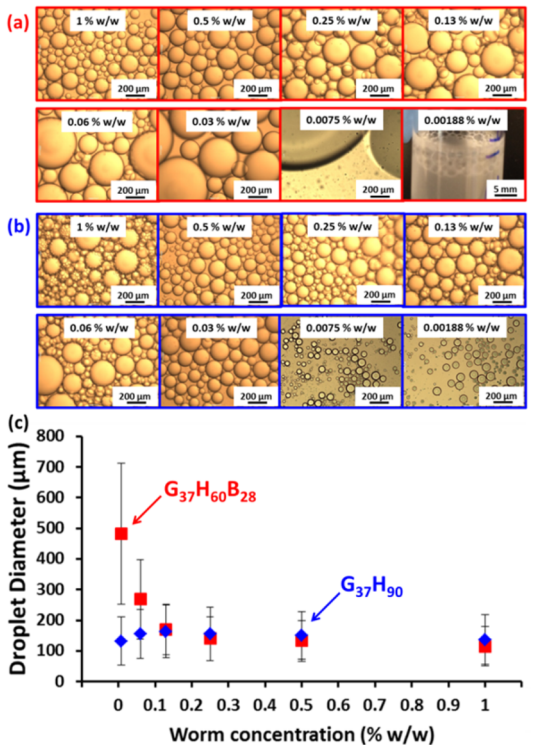

Figure 6. Optical microscopy images obtained for *n*-dodecane-in-water emulsion droplets prepared using either (a) $G_{37}H_{60}B_{28}$ or (b) $G_{37}H_{90}$ worms under low-shear conditions (i.e. hand-shaking). (c) Plots of mean droplet diameter (obtained by laser diffraction) vs worm concentration for emulsions prepared by hand-shaking dilute aqueous dispersions of $G_{37}H_{60}B_{28}$ worms (red, ■) and $G_{37}H_{90}$ worms (blue, ◆) with 20 vol % *n*-dodecane.

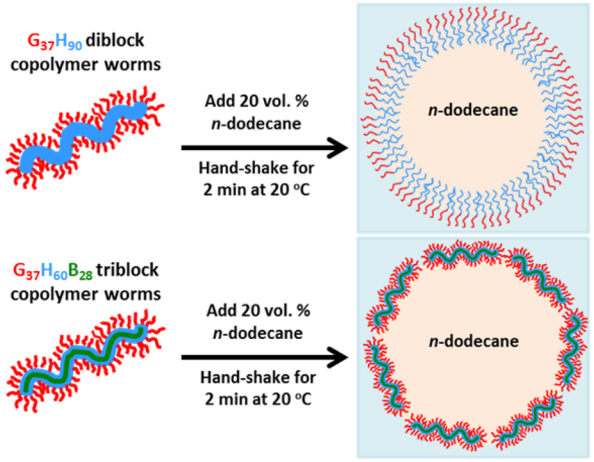

Figure 7. Schematic illustration of the attempted formation of Pickering emulsions using either $G_{37}H_{90}$ or $G_{37}H_{60}B_{28}$ worms under low-shear conditions (i.e., hand-shaking).

phobized silica particles reported by Arditty et al.[58] The instability observed in the present work suggests that worm desorption occurs; similar observations have been recently reported by Rizelli and co-workers for worm-stabilized Pickering non-aqueous emulsions.[59] In contrast, it is emphasized that the finer o/w emulsions prepared at higher worm concentrations (≥0.03% w/w) remain stable indefinitely.

Remarkably, both OM and laser diffraction studies indicated that the mean oil droplet diameter remained relatively constant on lowering the concentration of the $G_{37}H_{90}$ worms (Figures 6b and 6c). This indicates that these linear worms are so delicate that they cannot survive even low-shear hand-shaking. Instead, dissociation to form individual $G_{37}H_{90}$ copolymer chains occurs, which then adsorb at the oil−water interface to stabilize the oil droplets (see Figure 7). Again, mean oil droplet diameters were significantly larger (~136 μm) than those reported previously when using high-shear homogenization (~45 μm).

For emulsions stabilized using either $G_{37}H_{90}$ or $G_{37}H_{60}B_{28}$ worms, creaming of the low-density oil droplet phase occurred on standing for 24 h at 20 °C. The lower aqueous phase, which contained excess non-adsorbed copolymer, was carefully removed and analyzed by DLS to examine whether the worms remained intact after hand-shaking. DLS studies of the $G_{37}H_{90}$ aqueous phase indicated a hydrodynamic diameter of 41 nm (polydispersity = 0.18) and a much lower count rate (2500 kcps) than that observed for the original worms (37 000 kcps). This 93% reduction in count rate is fully consistent with substantial worm dissociation occurring during hand-shaking. In contrast, DLS studies of the aqueous phase removed from the $G_{37}H_{60}B_{28}$-stabilized emulsion indicated an apparent hydrodynamic diameter of 153 nm, a polydispersity of 0.23, and count rate of 21 000 kcps, which are comparable to the DLS data obtained before emulsification. These observations confirm that these $G_{37}H_{60}B_{28}$ worms remain intact after emulsification via hand-shaking.

Finally, closely related emulsions were prepared using *n*-hexane instead of *n*-dodecane to enable more convenient removal of the oil phase via evaporation at ambient temperature. Figure 8 shows TEM images obtained from emulsions prepared using the $G_{37}H_{60}B_{28}$ and $G_{37}H_{90}$ worms. In the latter case, the surface of the dried emulsion droplet is smooth and featureless, with no evidence for any adsorbed nanoparticles (see Figure 8a). Similar TEM observations were reported for both $G_{45}H_{150}$ diblock copolymer worms and $G_{45}H_{200}$ diblock copolymer vesicles in previous studies of shear-induced dissociation of diblock copolymer nano-objects.[36,54] In contrast, the dried emulsions prepared using the $G_{37}H_{60}B_{28}$ worms clearly comprise intact worms adsorbed at the oil−water interface (see Figure 8b). Thus all the experimental evidence suggests that, regardless of their morphology, G_xH_y nanoparticles are not sufficiently robust to survive emulsification under any conditions, even low-shear hand-shaking. However, incorporating highly hydrophobic PBzMA as a third block produces much more robust linear worms that can withstand high-shear homogenization and allow the formation of millimeter-sized emulsion droplets.

■ CONCLUSIONS

A series of PGMA−PHPMA−PBzMA triblock copolymer nano-objects have been prepared in concentrated aqueous solution via polymerization-induced self-assembly (PISA). For certain triblock compositions, highly anisotropic worm-like nanoparticles can be obtained with a mean contour length of 653 nm as determined by SAXS studies. Surprisingly, chain extension of the hydrophobic core-forming block of these worm-like nanoparticles does not lead to vesicle formation, with spherical micelles being formed instead. SAXS studies shed some light on these unexpected observations, which are best explained by considering changes in the relative enthalpic incompatibilities between the PGMA, PHPMA and PBzMA blocks during the *in situ* growth of the latter block. In particular,

DOI: 10.1021/acs.macromol.6b01729
Macromolecules 2016, 49, 7897−7907

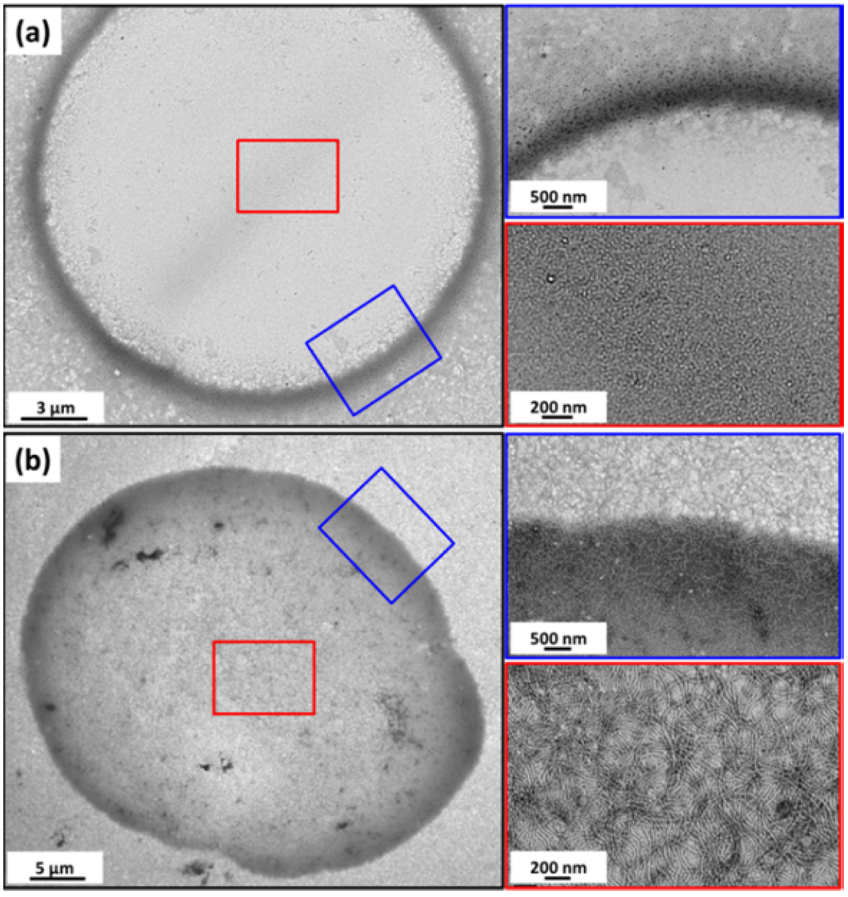

Figure 8. TEM images obtained for *n*-hexane-in-water emulsion droplets dried at 20 °C using (a) 0.25% w/w $G_{37}H_{90}$ diblock copolymer worms and (b) 0.25% w/w $G_{37}H_{60}B_{28}$ triblock copolymer worms. The edge (blue) and top surface (red) of the dried emulsion droplets are shown at higher magnification on the right-hand side. No worms are visible when using the $G_{37}H_{90}$ diblock copolymer since this undergoes dissociation even during low-shear homogenization (hand-shaking). In contrast, worms are clearly discernible when using the $G_{37}H_{60}B_{28}$ triblock copolymer, indicating that a genuine Pickering emulsion had been obtained.

SAXS data fits suggest that the effective R_g of the corona block actually increases as the PGMA−PHPMA diblock copolymer is chain-extended with BzMA, even though the same diblock precursor was used for all copolymer syntheses. Thus, at least some fraction of the partially hydrated PHPMA blocks must be gradually driven out of the increasingly hydrophobic core to become co-located with the hydrophilic PGMA stabilizer chains within the corona. SAXS analysis suggests that approximately one-third of the HPMA repeat units are displaced from the particle cores via this mechanism. This counterintuitive finding highlights the subtle switch from weak to strong segregation between incompatible blocks and its hitherto unappreciated effect on the evolution in copolymer morphology during PISA.

Finally, the PGMA−PHPMA−PBzMA triblock copolymer worms were evaluated as Pickering emulsifiers for *n*-dodecane oil droplets in water. Unlike the PGMA−PHPMA diblock copolymer worms reported previously, these triblock worms do not exhibit thermoresponsive behavior. However, they are much more robust when subjected to high-shear, which makes them much more effective Pickering emulsifiers. Low-shear emulsification (hand-shaking) enables the formation of metastable millimeter-sized oil droplets. Remarkably, the linear PGMA-PHPMA worms do not survive such mild shear conditions.

EXPERIMENTAL SECTION

Materials and Methods. *Materials.* All reagents were used as received unless otherwise stated. Benzyl methacrylate (BzMA), *n*-dodecane, 2-cyano-2-propyl benzodithioate (CPDB), and 4,4′-azobis-4-cyanopentanoic acid (ACVA) were purchased from Sigma-Aldrich (UK). BzMA inhibitor was removed by passing this monomer through an inhibitor removal column. Ethanol, dichloromethane, DMSO, and DMF were purchased from Fisher Scientific (UK). Glycerol monomethacrylate (GMA) was kindly donated by GEO Specialty Chemicals (Hythe) and used without further purification. 2-Hydroxypropyl methacrylate (HPMA) was purchased from Alfa Aesar (UK) and contained 0.07 mol % dimethacrylate impurity, as judged by high performance liquid chromatography (HPLC). Deuterated methanol (d_4-CD_3OD), dimethyl sulfoxide (d_6-DMSO), and dimethylformamide (d_7-DMF) NMR solvents were purchased from Goss Scientific (UK). Deionized water was obtained using an Elga Elgastat Option 3A water purifier; its pH was approximately 6.2, and its surface tension was 72.0 mN m^{-1} at 20 °C.

RAFT Synthesis of PGMA Macro-CTA Agent in Ethanol. The G_{37} macro-CTA was synthesized by Dr Vincent Ladmiral and the G_{92} macro-CTA was synthesized by Rheanna Perry, following previously reported protocols.[35]

Preparation of $G_{37}H_{60}$ Diblock Copolymer Precursor via RAFT Aqueous Solution Polymerization at 15% w/w Solids. G_{37} macro-CTA (5.00 g, 0.813 mmol), HPMA monomer (7.04 g, 48.8 mmol), deionized water (68.6 g), and ACVA (76.0 mg, 0.271 mmol, CTA/ACVA molar ratio = 3.0) were weighed into a 100 mL round-bottomed flask and purged with N_2 for 30 min prior to immersion in an oil bath set at 70 °C for 2 h. Finally, the polymerization was

DOI: 10.1021/acs.macromol.6b01729
Macromolecules 2016, 49, 7897−7907

quenched by cooling to room temperature with subsequent exposure to air.

Preparation of $G_{37}H_{60}B_z$ Triblock Copolymers (Where z Ranges from 10 to 550) via RAFT Seeded Emulsion Polymerization at 11−46% w/w Solids. Protocol for $G_{37}H_{60}B_{30}$ triblock copolymer worms: $G_{37}H_{60}$ diblock copolymer precursor (8.00 g of a 10% w/w copolymer solution, 1.00 g of copolymer, 0.0541 mmol), ACVA (3.03 mg, 0.0108 mmol, CTA/ACVA molar ratio = 5.0), and BzMA monomer (0. 286 g, 1.62 mmol, target DP = 30) were weighed into a 25 mL sample vial and purged with N_2 for 20 min prior to immersion in an oil bath set at 70 °C for 4 h. The polymerization was quenched by cooling to room temperature and subsequent exposure to air. This polymerization was conducted at 13% w/w solids. A series of similar copolymer syntheses were performed for which the PBzMA target DP ranged from 10 to 550 using BzMA masses varying from 0.0953 to 5.23 g (0.541 to 29.7 mmol), respectively, with the copolymer solids concentration increasing from 11 to 46% w/w.

Preparation of Linear $G_{37}H_{90}$ Diblock Copolymer Worms via RAFT Aqueous Dispersion Polymerization at 13% w/w Solids. G_{37} macro-CTA (1.00 g, 0.163 mmol), HPMA monomer (2.11 g, 14.6 mmol), deionized water (20.9 g), and ACVA (15.1 mg, 0.0542 mmol, CTA/ACVA molar ratio = 3.0) were weighed into a 50 mL round-bottomed flask and purged with N_2 for 30 min prior to immersion in an oil bath set at 70 °C for 2 h. Finally, the polymerization was quenched by cooling to room temperature with subsequent exposure to air.

Preparation of Linear $G_{92}B_{30}$ Diblock Copolymer Spheres via RAFT Aqueous Emulsion Polymerization at 13% w/w Solids. G_{92} macro-CTA (0.5 g, 0.0334 mmol), BzMA monomer (0.177 g, 1.00 mmol), deionized water (4.55 g), and ACVA (3.12 mg, 0.011 mmol, CTA/ACVA molar ratio = 3.0) were weighed into a 25 mL vial and purged with N_2 for 30 min prior to immersion in an oil bath set at 70 °C for 4 h. Finally, the polymerization was quenched by cooling to room temperature with subsequent exposure to air.

Pickering Emulsion Formation. Either *n*-dodecane or *n*-hexane (20 vol %) was shaken by hand with 2.0 mL of a 0.00188−1.0% w/w aqueous worm dispersion for 2 min at 20 °C. The droplets were imaged by OM, and the mean droplet diameter was determined by laser diffraction.

Copolymer Characterization. *^{1}H NMR Spectroscopy.* All NMR spectra were recorded using a 400 MHz Bruker Avance-400 spectrometer, and 64 scans were averaged per spectrum.

Gel Permeation Chromatography (GPC). Copolymer molecular weights and polydispersities were determined using a DMF GPC setup operating at 60 °C and comprising two Polymer Laboratories PL gel 5 μm Mixed C columns connected in series to a Varian 390 LC multidetector suite (only the refractive index detector was utilized) and a Varian 290 LC pump injection module. The GPC eluent was HPLC grade DMF containing 10 mM LiBr at a flow rate of 1.0 mL min^{-1}. DMSO was used as a flow-rate marker. Calibration was conducted using a series of ten near-monodisperse poly(methyl methacrylate) standards (M_n = 625−618 000 g mol^{-1}). The chromatograms were analyzed using Varian Cirrus GPC software (version 3.3) provided by the instrument manufacturer (Polymer Laboratories).

Dynamic Light Scattering (DLS). Intensity-average hydrodynamic diameters of the copolymer dispersions were determined using a Malvern Zetasizer NanoZS instrument. Dilute aqueous dispersions (0.10% w/w) were analyzed using disposable cuvettes, and all data were averaged over three consecutive runs to give the hydrodynamic diameter (D_h).

Transmission Electron Microscopy (TEM). As-synthesized copolymer dispersions were diluted at 20 °C to generate 0.10% w/w dispersions. Copper/palladium TEM grids (Agar Scientific) were surface-coated in-house to yield a thin film of amorphous carbon. The grids were then plasma glow-discharged for 30 s to create a hydrophilic surface. Individual samples of aqueous copolymer dispersions (0.1% w/w, 12 μL) were adsorbed onto the freshly glow-discharged grids for 20 s and then blotted with filter paper to remove excess solution. To stain the copolymer dispersions, uranyl formate (0.75% w/v) solution (9 μL) was soaked on the sample-loaded grid for 20 s and then carefully blotted to remove excess stain. The grids were then dried using a vacuum hose. Imaging was performed on a Phillips CM100 instrument at 100 kV, equipped with a Gatan 1 K CCD camera. A similar protocol was followed for the emulsion droplet grid preparation. The emulsion was shaken and a sample (12 μL) was adsorbed onto the freshly glow discharged grid. The grids were not blotted with filter paper to remove excess dispersion—instead, the hexane oil droplet evaporated after several minutes at ambient temperature. The staining protocol was the same as that for the aqueous copolymer dispersions.

Small-Angle X-ray Scattering (SAXS). SAXS patterns were recorded at Diamond Light Source (station I22, Didcot, UK). A monochromatic X-ray radiation (of wavelength λ = 0.1239 nm) and 2D SAXS detector (Pilatus 2M) were used for the experiment. The SAXS camera length setups covered the q range from 0.02 to 1.9 nm^{-1}, where $q = 4\pi \sin\theta/\lambda$ is the modulus of the scattering vector and θ is half of the scattering angle. A glass capillary cell of 1 mm thickness was used as the sample holder. X-ray scattering data were reduced by Dawn software and were further analyzed using Irena SAS macros for Igor Pro.[60] SAXS measurements were conducted on various aqueous dispersions, for which the copolymer concentration was diluted to 1.0% w/w for data collection. A scattering pattern of the homopolymer solution was collected using a laboratory SAXS instrument (a modified Bruker AXS Nanostar equipped with a microfocus Genix 3D Cu Kα radiation X-ray source and a collimator composed of two sets of motorized scatterless slits by Xenocs, a camera length of 1.46 m, and a 2D HiSTAR multiwire gas detector); glass capillaries of 2 mm diameter were used as a sample holder.

Rheology. An AR-G2 rheometer (TA Instruments) equipped with a variable temperature Peltier plate and a 40 mm 2° aluminum cone was used for all experiments. Percentage strain sweeps and angular frequency sweeps were conducted at 25 °C using a constant percentage strain of 1% and a constant angular frequency of 1 rad s^{-1}, respectively. The storage modulus and loss modulus were measured as a function of temperature at a fixed percentage strain (1%) and angular frequency (1 rad s^{-1}).

Optical Microscopy (OM). Optical microscopy images were recorded using a Motic DMBA300 digital biological microscope with a built-in camera and equipped with Motic Images Plus 2.0 ML software.

Laser Diffraction. A Malvern Mastersizer 2000 instrument equipped with a small volume Hydro 2000SM sample dispersion unit (ca. 50 mL), a HeNe laser operating at 633 nm, and a solid-state blue laser operating at 466 nm was used to size each emulsion. The stirring rate was adjusted to 1000 rpm in order to avoid creaming of the emulsion during analysis. After each measurement, the cell was rinsed once with ethanol, followed by three rinses with doubly distilled water; the glass walls of the cell were carefully wiped with lens cleaning tissue to avoid cross-contamination, and the laser was aligned centrally to the detector prior to data acquisition. The volume-average diameter was measured and repeated four times for each emulsion.

■ ASSOCIATED CONTENT

Supporting Information

The Supporting Information is available free of charge on the ACS Publications website at DOI: 10.1021/acs.macromol.6b01729.

DMF GPC curves, ^{1}H NMR spectra, extra SAXS patterns, rheology data, SAXS table of parameters, and SAXS models (PDF)

■ AUTHOR INFORMATION

Corresponding Author

*E-mail S.P.Armes@sheffield.ac.uk (S.P.A.).

Notes

The authors declare no competing financial interest.

DOI: 10.1021/acs.macromol.6b01729
Macromolecules 2016, 49, 7897−7907

■ ACKNOWLEDGMENTS

We thank Dr. Vincent Ladmiral and Rheanna Perry for the synthesis of the G_{37} and G_{92} macro-CTAs, respectively. Dr. V. J. Cunningham is acknowledged for conducting some additional ^{1}H NMR and UV GPC experiments. We thank Christopher Hill and Svetomir Tzokov at the University of Sheffield Biomedical Science Electron Microscopy Suite for their TEM assistance. The authors are grateful to Diamond (UK) for providing SAXS beam time. SPA thanks the European Research Council for an ERC Advanced Investigator grant (PISA 320372) to support C.J.M. and also EPSRC for a Platform grant (EP/J007846/1) to support M.J.D. and K.L.T.

■ REFERENCES

(1) Pickering, S. U. Emulsions. *J. Chem. Soc., Trans.* **1907**, *91*, 2001−2021.
(2) Levine, S.; Bowen, B. D.; Partridge, S. J. Stabilization of Emulsions by Fine Particles 1. Partitioning of Particles Between Continuous Phase and Oil-Water Interface. *Colloids Surf.* **1989**, *38* (4), 325−343.
(3) Binks, B. P.; Lumsdon, S. O. Stability of oil-in-water emulsions stabilised by silica particles. *Phys. Chem. Chem. Phys.* **1999**, *1* (12), 3007−3016.
(4) Binks, B. P.; Lumsdon, S. O. Effects of oil type and aqueous phase composition on oil-water mixtures containing particles of intermediate hydrophobicity. *Phys. Chem. Chem. Phys.* **2000**, *2* (13), 2959−2967.
(5) Binks, B. P.; Whitby, C. P. Silica Particle-Stabilized Emulsions of Silicone Oil and Water: Aspects of Emulsification. *Langmuir* **2004**, *20* (4), 1130−1137.
(6) Gautier, F.; Destribats, M.; Perrier-Cornet, R.; Dechezelles, J.-F.; Giermanska, J.; Heroguez, V.; Ravaine, S.; Leal-Calderon, F.; Schmitt, V. Pickering emulsions with stimulable particles: from highly- to weakly-covered interfaces. *Phys. Chem. Chem. Phys.* **2007**, *9* (48), 6455−6462.
(7) Binks, B. P.; Lumsdon, S. O. Pickering emulsions stabilized by monodisperse latex particles: Effects of particle size. *Langmuir* **2001**, *17* (15), 4540−4547.
(8) Thompson, K. L.; Armes, S. P.; York, D. W.; Burdis, J. A. Synthesis of Sterically-Stabilized Latexes Using Well-Defined Poly(glycerol monomethacrylate) Macromonomers. *Macromolecules* **2010**, *43* (5), 2169−2177.
(9) Thompson, K. L.; Armes, S. P.; Howse, J. R.; Ebbens, S.; Ahmad, I.; Zaidi, J. H.; York, D. W.; Burdis, J. A. Covalently Cross-Linked Colloidosomes. *Macromolecules* **2010**, *43* (24), 10466−10474.
(10) Walsh, A.; Thompson, K. L.; Armes, S. P.; York, D. W. Polyamine-Functional Sterically Stabilized latexes for Covalently Cross-linkable Colloidosomes. *Langmuir* **2010**, *26* (23), 18039−18048.
(11) Cauvin, S.; Colver, P. J.; Bon, S. A. F. Pickering Stabilized Miniemulsion Polymerization: Preparation of Clay Armored Latexes. *Macromolecules* **2005**, *38* (19), 7887−7889.
(12) Bon, S. A. F.; Colver, P. J. Pickering Miniemulsion Polymerization Using Laponite Clay as a Stabilizer. *Langmuir* **2007**, *23* (16), 8316−8322.
(13) Cui, Y.; Threlfall, M.; van Duijneveldt, J. S. Optimizing organoclay stabilized Pickering emulsions. *J. Colloid Interface Sci.* **2011**, *356* (2), 665−671.
(14) Cui, Y.; van Duijneveldt, J. S. Microcapsules Composed of Cross-Linked Organoclay. *Langmuir* **2012**, *28* (3), 1753−1757.
(15) Yang, Y.; Ning, Y.; Wang, C.; Tong, Z. Capsule clusters fabricated by polymerization based on capsule-in-water-in-oil Pickering emulsions. *Polym. Chem.* **2013**, *4* (21), 5407−5415.
(16) Thompson, K. L.; Fielding, L. A.; Mykhaylyk, O. O.; Lane, J. A.; Derry, M. J.; Armes, S. P. Vermicious thermo-responsive Pickering emulsifiers. *Chem. Sci.* **2015**, *6* (7), 4207−4214.
(17) Thompson, K. L.; Mable, C. J.; Lane, J. A.; Derry, M. J.; Fielding, L. A.; Armes, S. P. Preparation of Pickering Double Emulsions Using Block Copolymer Worms. *Langmuir* **2015**, *31* (14), 4137−4144.
(18) Noble, P. F.; Cayre, O. J.; Alargova, R. G.; Velev, O. D.; Paunov, V. N. Fabrication of "hairy" colloidosomes with shells of polymeric microrods. *J. Am. Chem. Soc.* **2004**, *126* (26), 8092−8093.
(19) Kalashnikova, I.; Bizot, H.; Cathala, B.; Capron, I. New Pickering Emulsions Stabilized by Bacterial Cellulose Nanocrystals. *Langmuir* **2011**, *27* (12), 7471−7479.
(20) Kalashnikova, I.; Bizot, H.; Cathala, B.; Capron, I. Modulation of Cellulose Nanocrystals Amphiphilic Properties to Stabilize Oil/Water Interface. *Biomacromolecules* **2012**, *13* (1), 267−275.
(21) Kalashnikova, I.; Bizot, H.; Bertoncini, P.; Cathala, B.; Capron, I. Cellulosic nanorods of various aspect ratios for oil in water Pickering emulsions. *Soft Matter* **2013**, *9* (3), 952−959.
(22) Wege, H. A.; Kim, S.; Paunov, V. N.; Zhong, Q.; Velev, O. D. Long-Term Stabilization of Foams and Emulsions with In-Situ Formed Microparticles from Hydrophobic Cellulose. *Langmuir* **2008**, *24* (17), 9245−9253.
(23) Madivala, B.; Vandebril, S.; Fransaer, J.; Vermant, J. Exploiting particle shape in solid stabilized emulsions. *Soft Matter* **2009**, *5* (8), 1717−1727.
(24) Blanazs, A.; Verber, R.; Mykhaylyk, O. O.; Ryan, A. J.; Heath, J. Z.; Douglas, C. W. I.; Armes, S. P. Sterilizable Gels from Thermo-responsive Block Copolymer Worms. *J. Am. Chem. Soc.* **2012**, *134*, 9741−9748.
(25) Semsarilar, M.; Jones, E. R.; Blanazs, A.; Armes, S. P. Efficient Synthesis of Sterically-Stabilized Nano-Objects via RAFT Dispersion Polymerization of Benzyl Methacrylate in Alcoholic Media. *Adv. Mater.* **2012**, *24* (25), 3378−3382.
(26) Fielding, L. A.; Derry, M. J.; Ladmiral, V.; Rosselgong, J.; Rodrigues, A. M.; Ratcliffe, L. P. D.; Sugihara, S.; Armes, S. P. RAFT dispersion polymerization in non-polar solvents: facile production of block copolymer spheres, worms and vesicles in n-alkanes. *Chem. Sci.* **2013**, *4* (5), 2081−2087.
(27) Cunningham, V. J.; Alswieleh, A. M.; Thompson, K. L.; Williams, M.; Leggett, G. J.; Armes, S. P.; Musa, O. M. Poly(glycerol monomethacrylate)−Poly(benzyl methacrylate) Diblock Copolymer Nanoparticles via RAFT Emulsion Polymerization: Synthesis, Characterization, and Interfacial Activity. *Macromolecules* **2014**, *47* (16), 5613−5623.
(28) Warren, N. J.; Mykhaylyk, O. O.; Ryan, A. J.; Williams, M.; Doussineau, T.; Dugourd, P.; Antoine, R.; Portale, G.; Armes, S. P. Testing the Vesicular Morphology to Destruction: Birth and Death of Diblock Copolymer Vesicles Prepared via Polymerization-Induced Self-Assembly. *J. Am. Chem. Soc.* **2015**, *137* (5), 1929−1937.
(29) Won, Y.-Y.; Davis, H. T.; Bates, F. S. Giant Wormlike Rubber Micelles. *Science* **1999**, *283* (5404), 960−963.
(30) Verber, R.; Blanazs, A.; Armes, S. P. Rheological studies of thermo-responsive diblock copolymer worm gels. *Soft Matter* **2012**, *8* (38), 9915−9922.
(31) Jones, E. R.; Semsarilar, M.; Blanazs, A.; Armes, S. P. Efficient Synthesis of Amine-Functional Diblock Copolymer Nanoparticles via RAFT Dispersion Polymerization of Benzyl Methacrylate in Alcoholic Media. *Macromolecules* **2012**, *45* (12), 5091−5098.
(32) Fielding, L. A.; Lane, J. A.; Derry, M. J.; Mykhaylyk, O. O.; Armes, S. P. Thermo-responsive Diblock Copolymer Worm Gels in Non-polar Solvents. *J. Am. Chem. Soc.* **2014**, *136* (15), 5790−5798.
(33) Derry, M. J.; Fielding, L. A.; Armes, S. P. Industrially-relevant polymerization-induced self-assembly formulations in non-polar solvents: RAFT dispersion polymerization of benzyl methacrylate. *Polym. Chem.* **2015**, *6* (16), 3054−3062.
(34) Blanazs, A.; Madsen, J.; Battaglia, G.; Ryan, A. J.; Armes, S. P. Mechanistic Insights for Block Copolymer Morphologies: How Do Worms Form Vesicles? *J. Am. Chem. Soc.* **2011**, *133* (41), 16581−16587.
(35) Blanazs, A.; Ryan, A. J.; Armes, S. P. Predictive Phase Diagrams for RAFT Aqueous Dispersion Polymerization: Effect of Block Copolymer Composition, Molecular Weight, and Copolymer Concentration. *Macromolecules* **2012**, *45* (12), 5099−5107.

DOI: 10.1021/acs.macromol.6b01729
Macromolecules 2016, 49, 7897−7907

(36) Thompson, K. L.; Mable, C. J.; Cockram, A.; Warren, N. J.; Cunningham, V. J.; Jones, E. R.; Verber, R.; Armes, S. P. Are block copolymer worms more effective Pickering emulsifiers than block copolymer spheres? *Soft Matter* **2014**, *10* (43), 8615−8626.
(37) Warren, N. J.; Armes, S. P. Polymerization-Induced Self-Assembly of Block Copolymer Nano-objects via RAFT Aqueous Dispersion Polymerization. *J. Am. Chem. Soc.* **2014**, *136* (29), 10174−10185.
(38) Pedersen, J. S. Form factors of block copolymer micelles with spherical, ellipsoidal and cylindrical cores. *J. Appl. Crystallogr.* **2000**, *33* (3−1), 637−640.
(39) Pedersen, J. S.; Schurtenberger, P. Scattering Functions of Semiflexible Polymers with and without Excluded Volume Effects. *Macromolecules* **1996**, *29* (23), 7602−7612.
(40) Cunningham, V. J.; Ratcliffe, L. P. D.; Blanazs, A.; Warren, N. J.; Smith, A. J.; Mykhaylyk, O. O.; Armes, S. P. Tuning the critical gelation temperature of thermo-responsive diblock copolymer worm gels. *Polym. Chem.* **2014**, *5* (21), 6307−6317.
(41) Fetters, L. J.; Lohse, D. J.; Colby, R. H. Chain Dimensions and Entanglement Spacings In *Physical Properties of Polymers Handbook*; Mark, J., Ed.; Springer: New York, 2007; pp 447−454.
(42) Blanazs, A.; Armes, S. P.; Ryan, A. J. Self-Assembled Block Copolymer Aggregates: From Micelles to Vesicles and their Biological Applications. *Macromol. Rapid Commun.* **2009**, *30* (4−5), 267−277.
(43) Charleux, B.; Delaittre, G.; Rieger, J.; D'Agosto, F. Polymerization-Induced Self-Assembly: From Soluble Macromolecules to Block Copolymer Nano-Objects in One Step. *Macromolecules* **2012**, *45* (17), 6753−6765.
(44) Zhang, X.; Boissé, S.; Zhang, W.; Beaunier, P.; D'Agosto, F.; Rieger, J.; Charleux, B. Well-Defined Amphiphilic Block Copolymers and Nano-objects Formed in Situ via RAFT-Mediated Aqueous Emulsion Polymerization. *Macromolecules* **2011**, *44* (11), 4149−4158.
(45) Zhang, W.; D'Agosto, F.; Boyron, O.; Rieger, J.; Charleux, B. Toward a Better Understanding of the Parameters that Lead to the Formation of Nonspherical Polystyrene Particles via RAFT-Mediated One-Pot Aqueous Emulsion Polymerization. *Macromolecules* **2012**, *45* (10), 4075−4084.
(46) Glatter, O.; Kratky, O. *Small-Angle X-ray Scattering*; Academic Press: London, 1982.
(47) Pedersen, J. S.; Gerstenberg, M. C. Scattering Form Factor of Block Copolymer Micelles. *Macromolecules* **1996**, *29* (4), 1363−1365.
(48) Israelachvili, J. N.; Mitchell, D. J.; Ninham, B. W. Theory of self-assembly of hydrocarbon amphiphiles into micelles and bilayers. *J. Chem. Soc., Faraday Trans. 2* **1976**, *72* (0), 1525−1568.
(49) NMR spectroscopy studies were performed in D_2O in order to attempt to monitor any changes in the degree of solvation of the core-forming PHPMA block as a function of target DP of the PBzMA block. *In situ* ^{1}H NMR experiments in D_2O were also conducted, whereby the PGMA−PHPMA diblock copolymer precursor was chain-extended with BzMA. Unfortunately, the PGMA and PHPMA signals were poorly resolved in all cases, which prevented meaningful quantitative analysis. Thus, ^{1}H NMR spectroscopy cannot be used to assess changes in the relative degree of hydration of the PHPMA block in this particular case.
(50) Hammouda, B. *Probing Nanoscale Structures - The SANS Toolbox*; National Institute of Standards and Technology: 2008.
(51) Mable, C. J.; Warren, N. J.; Thompson, K. L.; Mykhaylyk, O. O.; Armes, S. P. Framboidal ABC triblock copolymer vesicles: a new class of efficient Pickering emulsifier. *Chem. Sci.* **2015**, *6* (11), 6179−6188.
(52) Growney, D. J.; Mykhaylyk, O. O.; Derouineau, T.; Fielding, L. A.; Smith, A. J.; Aragrag, N.; Lamb, G. D.; Armes, S. P. Star Diblock Copolymer Concentration Dictates the Degree of Dispersion of Carbon Black Particles in Nonpolar Media: Bridging Flocculation versus Steric Stabilization. *Macromolecules* **2015**, *48* (11), 3691−3704.
(53) Lee, A. S.; Gast, A. P.; Bütün, V.; Armes, S. P. Characterizing the Structure of pH Dependent Polyelectrolyte Block Copolymer Micelles. *Macromolecules* **1999**, *32* (13), 4302−4310.
(54) Thompson, K. L.; Chambon, P.; Verber, R.; Armes, S. P. Can Polymersomes Form Colloidosomes? *J. Am. Chem. Soc.* **2012**, *134* (30), 12450−12453.
(55) Binks, B. P.; Lumsdon, S. O. Influence of Particle Wettability on the Type and Stability of Surfactant-Free Emulsions. *Langmuir* **2000**, *16* (23), 8622−8631.
(56) Binks, B. P. Particles as surfactants - similarities and differences. *Curr. Opin. Colloid Interface Sci.* **2002**, *7* (1−2), 21−41.
(57) Aveyard, R.; Binks, B. P.; Clint, J. H. Emulsions stabilised solely by colloidal particles. *Adv. Colloid Interface Sci.* **2003**, *100−102*, 503−546.
(58) Arditty, S.; Whitby, C. P.; Binks, B. P.; Schmitt, V.; Leal-Calderon, F. Some general features of limited coalescence in solid-stabilized emulsions. *Eur. Phys. J. E: Soft Matter Biol. Phys.* **2003**, *11* (3), 273−281.
(59) Rizzelli, S. L.; Jones, E. R.; Thompson, K. L.; Armes, S. P. Preparation of non-aqueous Pickering emulsions using anisotropic block copolymer nanoparticles. *Colloid Polym. Sci.* **2016**, *294* (1), 1−12.
(60) Ilavsky, J.; Jemian, P. R. Irena: tool suite for modeling and analysis of small-angle scattering. *J. Appl. Crystallogr.* **2009**, *42*, 347−353.

DOI: 10.1021/acs.macromol.6b01729
Macromolecules 2016, 49, 7897−7907